



HAL
open science

Porous 3D Cu structures with adaptive heat dissipation properties

Jean-François Silvain, Helies Boumali, Julie Bourret, Pierre-Marie Geffroy, Sébastien Fourcade, Thomas Batigne, Karim Sinno, Yongfeng Lu, Loic Constantin

► **To cite this version:**

Jean-François Silvain, Helies Boumali, Julie Bourret, Pierre-Marie Geffroy, Sébastien Fourcade, et al.. Porous 3D Cu structures with adaptive heat dissipation properties. MRS Communications, 2022, 12, pp.753-758. 10.1557/s43579-022-00224-2 . hal-03761379

HAL Id: hal-03761379

<https://hal.science/hal-03761379>

Submitted on 26 Aug 2022

HAL is a multi-disciplinary open access archive for the deposit and dissemination of scientific research documents, whether they are published or not. The documents may come from teaching and research institutions in France or abroad, or from public or private research centers.

L'archive ouverte pluridisciplinaire **HAL**, est destinée au dépôt et à la diffusion de documents scientifiques de niveau recherche, publiés ou non, émanant des établissements d'enseignement et de recherche français ou étrangers, des laboratoires publics ou privés.

Porous 3D Cu structures with adaptive heat dissipation properties

Jean-François Silvain^{a,d,*}, Helies Boumali^a, Julie Bourret^b, Pierre-Marie Geffroy^b,
Sebastien Fourcade^a, Thomas Batigne^c, Karim Sinno^c, Yongfeng Lu^d, and Loic
Constantin^{a,d}

^a *Institut de Chimie de la Matière Condensée de Bordeaux, ICMCB, UMR 5026, University of Bordeaux, CNRS, Bordeaux INP, 87 Avenue du Docteur Schweitzer 33600 Pessac, France*

^b *Institute of Research for Ceramics, IRCER, CNRS, Université de Limoges, CEC, 12 Rue Atlantis, 87068 Limoges, France*

^c *Lynxter, 9 rue Pierre Georges Latecoere, 64100 Bayonne, France*

^d *Department of Electrical and Computer Engineering, University of Nebraska-Lincoln, Lincoln, NE 68588-0511, USA*

*Corresponding author: jean-francois.silvain@icmcb.cnrs.fr

Abstract

This study focuses on the formulation of copper paste with optimal properties to micro-extrude porous Cu heat sinks, using extrusion additive manufacturing. The influence of the debinding and sintering conditions on the porosity level and the heat dissipation behavior have been investigated. Open air debinding leads to a density increases from 200 up to 400 °C, then decreases from 400 down to 600 °C. This behavior is a result from a competition between densification and the oxidation. Heat dissipation of the copper heat sink increases in respect to the porosity ratio of the sintered part.

Keywords: 3D printing; Cu; debinding; sintering; Additive manufacturing; thermal conductivity

28 **1. Introduction**

29 With the emerging of new technologies, the field of transport tends to rely more on electrical systems, such
30 as auxiliary controls as well as traction requirements. The aerospace industry is turning to the manufacture of
31 more electric planes, which allow better management of the rationalization / management of energy on board.
32 The increasing share of electricity in airplanes reduces fuel consumption, cuts costs and maintenance time. As
33 a result, the electrical power used on board in transport systems is increasingly important. During operation,
34 electronic systems undergo thermal gradients, which generate thermomechanical stresses at the interfaces
35 between these different layers of electronic systems. These interfacial stresses, induced by the differences in
36 thermal expansion coefficient between the different layers, then produce thermal fatigue, which leads to
37 irreversible physical degradation of the system. The on-board electronic components are also temperature
38 sensitive and have temperature limits for reliable operations (e.g., ~140 °C maximum for silicon). The heat
39 dissipation in these components is essential to ensure an operating temperature below this maximum
40 temperature. Thus, cooling systems have been then developed by several teams around the world to increase
41 the heat dissipation performance through studying new materials and geometries [1-3].

42 Constantin et. al [4] has shown that increasing the specific surface area of a material improves the heat
43 dissipation properties of the same material. So, two strategies can be envisioned through: 1) producing
44 complex shapes in order to obtain parts with a large specific surface area, and 2) developing materials
45 intrinsically having larger specific surface areas (i.e., porous materials).

46 The high thermal conductivity (~ 400 W/mK) of pure copper (Cu) makes it an essential material for thermal
47 management in numerous industries, such as microelectronics, power plants, and aerospace [5-7]. However,
48 the shape (*i.e.*, surface area) of heat sinks, playing a crucial role in heat dissipation, is limited to simple
49 geometries in current fabrication techniques [8-9].

50 For obtaining exceptional properties, many methods of producing porous metals have been developed around
51 the world, such as sol-gel chemistry, the use of space-holders, and additive manufacturing [10]. The latter is
52 a layer-by-layer approach allowing quick and cost-effective manufacturing of highly complex parts in small
53 quantities without the necessity of specific tools. Using porous structures in manufacturing has a few
54 advantages, including the cost reduction as compared to the powder bed fusion as compared to other
55 technologies such as inkjet or thermoplastic extrusion in which non eco-friendly binders are used.

56 The main objective of the study is to obtain porous materials by 3D printing, using an extrusion additive
57 manufacturing (EAM) method and eco-friendly paste, to convert pastes to porous structures with ideal heat
58 dissipation properties. Initially, pastes with properties suitable for micro-extrusion are formulated. The pastes
59 must be sufficiently fluid to be extruded, but sufficiently viscous to hold the shapes during the printing process
60 (extrusion and drying) and post treatment (debinding and sintering). For this purpose, the nature of the binder
61 together with the morphology of the fillers and their volume percentage are controlled. The formulation of the

Cu pastes was based on the work by J. Bourret *et al.* [11] using eco-friendly additives. The binder and pastes were characterized macroscopically. The powders are characterized by X-ray diffraction, scanning electron microscopy, and laser granulometry. Secondly, to control porosity, regular parts were printed to study the impact of heat treatments (debinding, sintering) on the structure and microstructure of the parts, which will be characterized. Finally, the physical properties of parts with controlled porosity were studied by heat dissipation and Vickers hardness.

2. Experimental method

2.1. Preparation of the Cu paste

The Cu pastes were prepared using a spherical Cu powder (ECKA[®] Granules (Germany, GmbH) with a medium particle size d_{50} close to 20 μm . Glycerol (Alfa Aesar A16205.AP, Thermo Fisher GmbH, Germany) was used as a plasticizer. The binder was obtained by acoustic mixing during 3 minutes (Labram, Resodyn, USA) of 5 wt.% of a water-soluble polysaccharide powder with distilled water as a solvent. This polysaccharide is eco-friendly and found in a wide range of applications thanks in part to its thickening, stabilizing, gelling and binding properties: food, cosmetic, medical and pharmaceutical industries [12]. Their nontoxicity, life cycles and low cost make them ideal natural additives. Due to its high hydrophilic properties, it is able to form a network due to the swelling of their particles [13]. After preparation, pseudo-gels are obtained and were kept in the refrigerator at 8 °C for around 24 hours.

Cu powders were introduced into a container with the pseudo-gel at room temperature (binder + plasticizer). The Cu pastes were prepared by mixing all these components in an acoustic mixer for 3 minutes. Once mixing was finished, the Cu paste was then kept in the refrigerator at 8 °C for a minimum of 24 hours of rest before being used in micro-extrusion. In our study, the formulation for the micro-extrusion contains 50 vol.% of Cu particles. This ratio corresponds to a best compromise between suitable rheological properties of the paste (with low viscosity) and the maximum ratio of metallic particles in the extrusion paste [11].

2.2. 3D printing

The micro-extrusion tests have been performed with a 3D printer (S600D, Lynxter, Bayonne, France) with the PAS11 tool head. Simple 3D cubes (10x10x10 mm³) parts were obtained from a CAD file; sliced using a software (Simplify 3D) to obtain the printing path with the computer G-code language executed by the printer. The diameter of the nozzle and the distance between 2 strands are equal to 0.86 mm.

2.3. Consolidation by heat treatments

After extrusion, the parts were dried at room temperature and then debinded and sintered. Nabertherm RD

30/200/11 tube furnace is used for debinding and sintering. To determine the debinding cycle, thermal analysis was carried out on the binder powder. Several dwell temperatures of debinding ($T^{\circ} = 300, 400, 500,$ and $600\text{ }^{\circ}\text{C}$) in air and argon (Ar), with a flow of 200 mL/min , were tested to evaluate the impact of these parameters on the parts' density and microstructure. However, the heating ramp was fixed at $5\text{ }^{\circ}\text{C/min}$ with a dwell time of 1 hour.

Sintering was used to obtain parts with a density lower than 60% to maximize specific surface areas with optimized thermal dissipation. Sintering was performed at $700\text{ }^{\circ}\text{C}$ for 60 min in an Ar/H₂(5%) atmosphere with a flow of 200 mL/min . The heating ramp is equal to $6\text{ }^{\circ}\text{C/min}$ with a dwell time of 2 hours.

2.4. Structural and micro-structural characterization

The Archimedes method (Mettler Toledo AT201) was used to measure the real density of the samples and the mercury intrusion porosimeter to measure the pore volume and porosity of the Cu materials. The relative density was calculated by dividing the real density by the theoretical density of Cu, CuO and Cu₂O ($d_{\text{Cu}} = 8.96\text{ g/cm}^3$, $d_{\text{CuO}} = 6.31\text{ g/cm}^3$, $d_{\text{Cu}_2\text{O}} = 6\text{ g/cm}^3$) knowing the amount of Cu, CuO and Cu₂O inside the densified materials. The microstructure of printed parts was analyzed by Scanning Electron Microscopy (SEM, VEGA II SBH, TESCAN). The surface area is the main factor in thermal management. To demonstrate the benefit of additive manufacturing in thermal management, the heat dissipation performance of different structures printed was measured and compared to a dense Cu. In the experimental set-up [4], the heat sink was attached to a memory card chip placed on a hot plate heated to $200\text{ }^{\circ}\text{C}$. A fan was located 10 cm from the top of the heat sink to produce an airflow. The temperature of the electronic chip was measured using an IR camera about 0.5 m from the heat sink with a precision of $\pm 2\text{ }^{\circ}\text{C}$.

3. Results and discussion

3.1 Debinding of the Cu materials printed

The diffractograms in Figure 1 show that during debinding under argon, whatever the debinding temperature, the structure of the parts is identical to that of the starting powder; it is highly crystallized cubic copper with well-defined peaks. On the other hand, when debinding is carried out in air, the structure evolves. CuO and Cu₂O peaks appear from $200\text{ }^{\circ}\text{C}$.

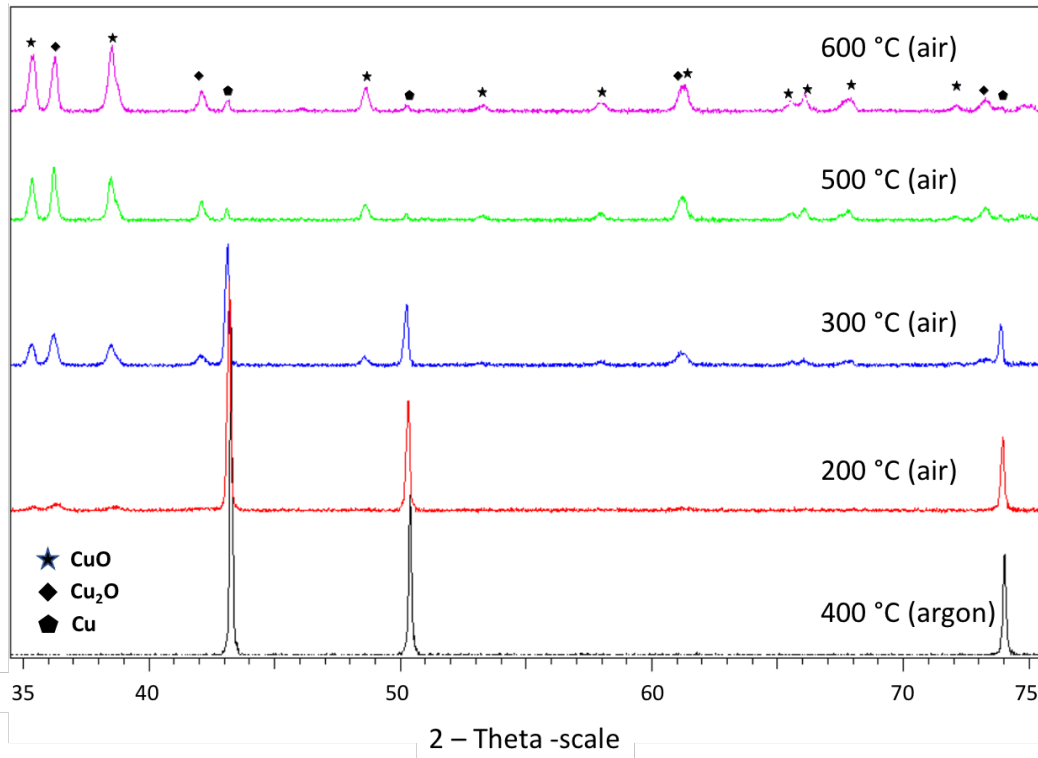


Figure 1: Typical diffraction diagram of Cu materials debinding under argon and air atmosphere at different temperature

The predominance of the phases has been plotted as a function of the debinding temperature in air in Figure 2. Figure 2a shows that when the debinding temperature increases, the Cu phase is gradually consumed in favor of the oxide phases; it is completely consumed at 600°C. The proportion of the Cu₂O phase stabilizes between 20 and 30% while the CuO phase becomes predominant at 525°C. The Cu₂O phase does not increase because it serves as a reaction intermediate for the formation of the CuO phase.

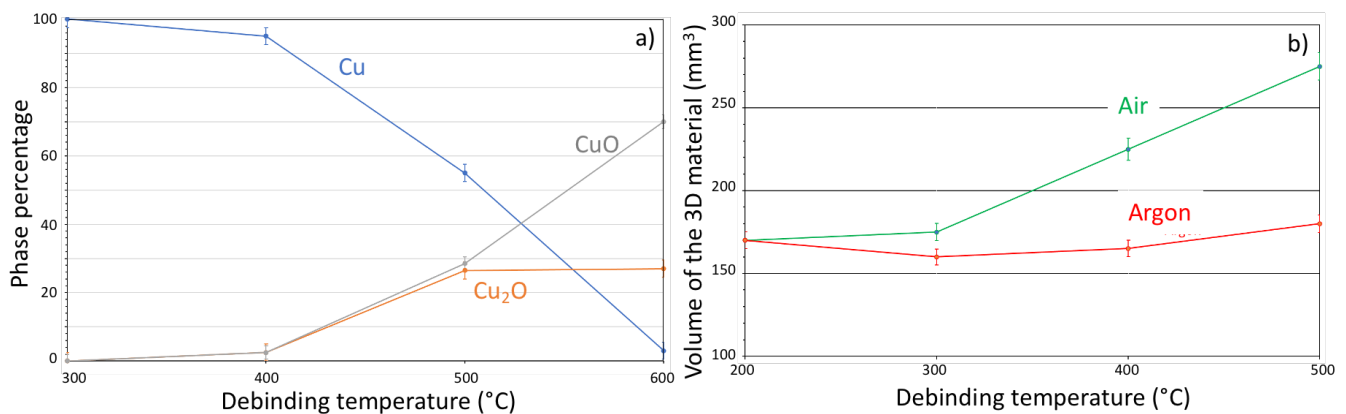


Figure 2: Evolution of a) the chemical composition, with air debinding temperature, of the Cu materials and, b) the volume of the materials, in mm³ of the Cu materials at different air debinding temperatures

In Fig. 2b, it notes the variation of the Cu part volume in mm³, in relation with the debinding temperature. As it can be seen in the Fig. 2a, the concentration of Cu oxide increases for a temperature greater than 300 °C and therefore shows the transformation of metal Cu to two different Cu oxides, Cu₂O and CuO. Cu oxides have lattice parameters greater than that of pure Cu; this induces volume differences in the unit cell: $V_{\text{Cu}} = 47.24 \text{ \AA}$, $V_{\text{Cu}_2\text{O}} = 77.83 \text{ \AA}$ and $V_{\text{CuO}} = 81.22 \text{ \AA}$ [15]. These variations of the cell volume induced the increasing of the volume of the Cu parts during the debinding under air. Fig. 2b shows that for the parts debinded in argon, the volume is quite stable up to 400 °C and slightly increase after this temperature. For parts debinded in air, the volume of the parts is almost stable up to 300 °C, and then increases afterwards. This behavior results from a competition between two phenomena: A first phenomenon of densification caused by pre-sintering of Cu particles is preponderant up to 300 °C. For temperature higher than 300 °C, oxidation of Cu is predominant. This observation agrees with the micrography in Fig. 3a which shows that there is no visible evolution of the Cu powders after a heat treatment under Argon, which compare with the same temperature under air (cf. Fig. 3b and 3c). Fig. 3c shows the growth of nanowires on top of the Cu particles. The CuO nanowires start appearing when the temperature reaches 400 °C and grow continuously as the annealing time increases. It is assumed that the formation of these CuO nanowires is driven by the thermal oxidation of Cu during annealing [15]. Such a phenomenon has already been observed by Jiang et al. [16]. A step-by-step kinetic study of the growth process shows that the CuO nanowires start appearing when the temperature reaches 400 °C and grow continuously as the annealing time increases, reaching lengths of several microns after 2 h of annealing. It is assumed that the formation of these CuO nanowires is driven by the thermal oxidation of copper during annealing. Cuprous oxide (Cu₂O) is known to be the first product of Cu oxidation, while CuO is formed in a second step. Many mechanisms have been proposed in order to explain this phenomenon, such as the catalytic action of Cu₂O on CuO formation through a vapor–solid mechanism [16], or the growth stresses in the oxide layers strong enough to extrude CuO wires from the surface [17].

The evolution of the microstructure, for material with a debinded in air, is correlated to the formation of Cu oxide. In contrary, the microstructures of the Cu parts with debinding in Ar, are quite similar at any debinding temperatures due to the absence of the Cu oxidation in Ar atmosphere.

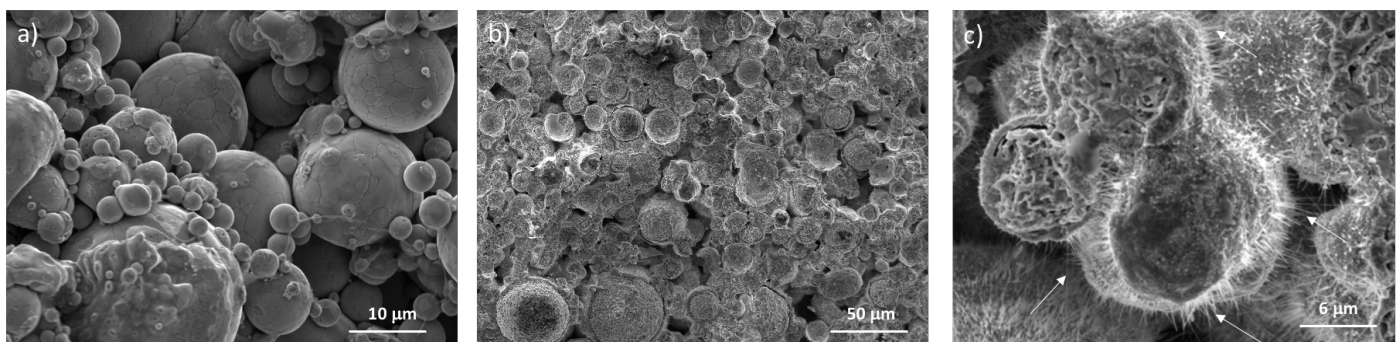


Figure 3: SEM microstructure of the Cu materials debinded at 400 °C under a) Ar, and b, c) air (white arrows shows CuO nanowires)

Fig. 4a shows that debinding conditions have a significant impact on the final sample density. For samples debinded in air, as the debinding temperature increases, the density of the parts increases from 200 to 400 °C, then decreases from 400 to 600 °C. This behavior results from a competition between the densification caused by the sintering (decrease of the porosity inside the material) and the formation of Cu oxide (Cu_2O and CuO), which have a density lower than pure Cu. When the samples are debinded in Ar, there is no Cu oxide formation; the density of the parts therefore increases linearly with the sintering temperature. Above 400 °C, the decrease of the measured density for Cu material debinded in air has to be correlated with the increase of the CuO and Cu_2O percentage.

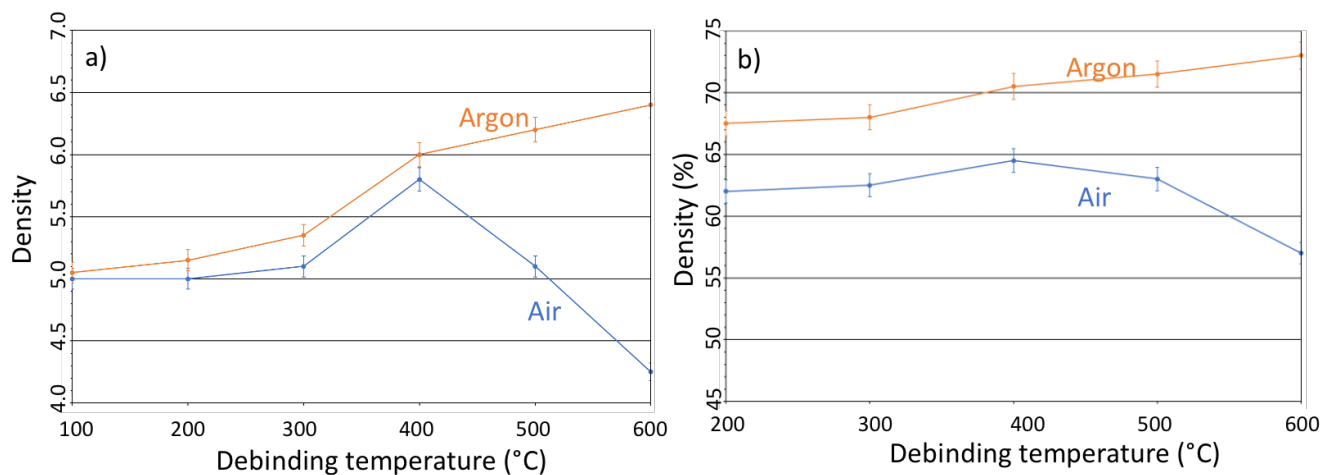


Fig. 4: Evolution of the porosity level, inside the Cu material, after a) 60 min debinding in air and Ar atmosphere and b) debinding and sintering at 700 °C for 60 min in an $\text{Ar}/\text{H}_2(5\%)$ atmosphere.

3.2 Sintering of the Cu materials printed

After debinding at different temperatures and atmospheres, Fig. 4b shows the evolution of the density of the sintered at 700 °C for 60 min in an $\text{Ar}/\text{H}_2(5\%)$ atmosphere. First, the sintered densities are higher for materials debinded in air than those debinded under Ar at any temperature. Second, the variation of the density of the sintered materials shows the same trend that the variation of just debinded material. For samples debinded in air, an increase in the density is observed first for temperatures up to 400 °C, followed by a decrease at higher temperatures. For samples debinded in Ar, a continuous increase can be observed.

3.3 Heat dissipation of the materials 3D printed

Fig. 5 shows the evolution of the temperature difference between the hot plate and the electronic chip as a function of the porosity level of the sintered Cu parts. It has to be mentioned that, for this paper, just selective

materials with micrometric porosity, induced by different debinding temperature and sintering conditions, ranging from 5 to 30% have been analyzed. All of these materials have been debinded under air. In a future paper, macro porosities, induced by EAM process, will be associate with micro porosities in order to increase the porosity range and to see the effect of the porosity size and shape with the thermal dissipation behavior. The heat dissipation in the porous Cu part significantly depends on the porosity level inside the Cu part sintered. Ended, when the volume fraction of pores increases, the temperature difference between the hot plate and the electronic chip increases and so does the ability of the porous Cu to dissipate heat. Therefore, it is possible to improve the heat dissipation of a material by increasing its specific surface areas through a higher porosity. It has to be mentioned that, due to the fact that the porosity level inside the sinter Cu materials is much higher than 5%, the structure porosity must be consider has open. This open porosity allows a better dissipation of the heat on the surface and inside the Cu parts.

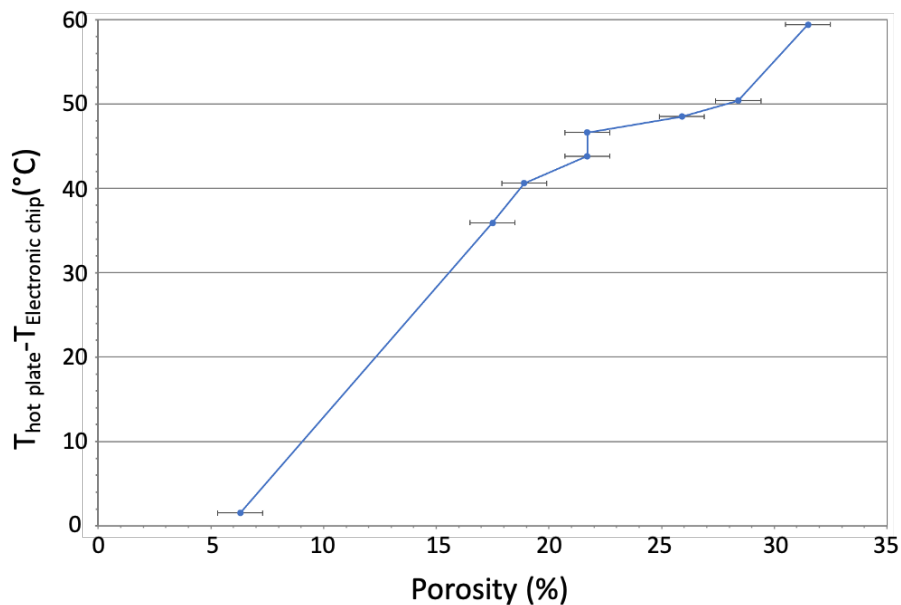


Figure 5: Evolution of the temperature difference between the hot plate and the electronic chip in function of the porosity level of the Cu materials.

4. Conclusion

Cu pastes with optimal properties for micro-extrusion have been formulated and porous Cu materials have been fabricated by 3D printing, using the EAM method. The influence of the debinding and sintering conditions (atmosphere, temperature, and time) on the porosity level and the heat dissipation behavior have been investigated. The results could be summarized as follows.

- 1) Debinding conditions have a significant impact on sample density. For samples debinded in air the density of the parts increases from 200 to 400 °C, then decreases from 400 to 600 °C. This behavior

214 results from a competition between the densification induced by the sintering and the Cu oxidation.
215 When the samples are debinded in Ar, there is no oxide formation. Cu parts debinded in air are more
216 porous than those in argon.

- 217 2) The variation of the density of the sintered materials show the same trend that the variation of just
218 debinded material. For the samples debinded in air, an increase in the density is observed up to 400
219 °C, followed by a decrease at higher temperatures.
- 220 3) For Cu materials, the porosity level inside the materials 3D fabricated can be controlled by changing
221 the debinding and sintering conditions.
- 222 4) Heat dissipation of the porous Cu part strongly depends on the porosity level inside the sintered Cu
223 parts. For such open porosity structure, the increase of the volume fraction of pores is strictly correlated
224 with the ability of the porous Cu to dissipate heat.
- 225 5) Finally, this innovative work shows clearly that the EAM method, using eco-friendly paste, can be a
226 promising method to product the heat sink with a very heat dissipation ability thank to a specific
227 internal porosity of material sintered and also the specific 3D shape of Cu heat sink.

228 ***Acknowledgments***

229 The authors would like to thanks Eric Lebraud of the Institut de Chimie de la Matière Condensée de Bordeaux
230 for performing the XRD analyses.
231

232 ***Declarations of interest***

233 None
234

235 ***Data availability***

236 All data generated or analyzed during this study are included in this published article
237
238

239 ***Funding***

240 This research did not receive any specific grant from funding from funding agencies in the public, commercial,
241 or not-for-profit sectors.
242

243 ***References***

244 [1] Y. Cui, Z. Qin, H. Wu, M. Li, Y. Hu, Nature Communications 12(1), 4457 (2021)

245 [2] Y. Li, L. Gong, M. Xu, Y. Joshi, Journal of Electronic Packaging, Transactions of the ASME 143(3), (2021)

- 246 [3] M. Baldry, V. Timchenko, C. Menictas, *Journal of Thermal Science and Engineering Applications* 13(4),
247 41001 (2021)
- 248 [4] L. Constantin, L. Fan, Z. Wu, B. Mortaigne, J.-F. Silvain, YF Lu, *Laser 3D printing of complex Copper*
249 *structures*, *Additive Manufacturing* 35, 101268 (2020)
- 250 [5] F. Singer, D.C. Deisenroth, D.M. Hymas, M.M. Ohadi, 16th IEEE Intersociety Conference on Thermal and
251 Thermomechanical Phenomena in Electronic Systems (ITherm), 174 (2017)
- 252 [6] C. Körner, *International Materials Reviews* 61, 361 (2016)
- 253 [7] J.-F. Silvain, J.-M. Heintz, A. Veillere, L. Constantin, YF Lu, *Int. J. Extrem. Manuf.* 2, 012002 (2019)
- 254 [8] H. Zhang, L. Chen, Y. Liu, Y. Li, *International Journal of Heat and Mass Transfer* 56, 172 (2013)
- 255 [9] W.E. Frazier, *J. of Material Engineering and Perform* 23, 1917 (2014)
- 256 [10] D.K. Mishra, P.M. Pandey, *Materials Science & Engineering A* 804, 1407592021 (2021)
- 257 [11] J. Bourret, I. EL. Younsi, M. Bienia, A. Smith, P.-M. Geffroy, J. Marie, Y. Ono, T. Chartier, V. Pateloup,
258 *Journal of the European Ceramic Society* 38, 2802 (2018)
- 259 [12] N. Thombare, U. Jha, S. Mishra, M.Z. Siddiqui, *Int. J. Biol. Macromol.* 88, 361 (2016)
- 260 [13] R. Lapasin, S. Pricl, *Rheology of Industrial Polysaccharides: Theory and Applications*, First Edition,
261 Springer US, <https://doi.org/10.1007/978-1-4615-2185-3> (accessed March 25, 2020) (1995).
- 262 [14] L. Constantin, PhD thesis, University of Bordeaux (2020)
- 263 [15] J.-F. Silvain, C. Vincent, T. Guillemet, A. Veillere, J.-M. Heintz, *Material Research Bulletin* 47, 500
264 (2012)
- 265 [16] X. Jiang, T. Herricks, Y. Xia, *Nano Lett.* 2 (12), 1333 (2002)
- 266 [17] T. Homma, S. Issiki, *Acta Metall.* 12, 1092 (1964)
- 267